Received 20 November 2019; revised 30 December 2019; accepted 29 January 2020. Date of publication 14 April 2020; date of current version 12 May 2020.

*Digital Object Identifier 10.1109/OJAP.2020.2987929*

# Differentially-Fed Aperture-Coupled Magneto-Electric Dipole Antenna With Continuously Variable Beamwidth

**YUAN JI [1] (Graduate Student Member, IEEE), LEI GE [2] (Senior Member, IEEE), JIANPENG WANG [1], QUANGANG CHEN [3], AND WEN WU [1] (Senior Member, IEEE)**

[1]Ministerial Key Laboratory of JGMT, Nanjing University of Science and Technology, Nanjing 210094, China

[2]College of Electronic and Information Engineering, Shenzhen University, Shenzhen 518060, China

[3]School of Electrical Engineering, Aalto University, 00076 Espoo, Finland

CORRESPONDING AUTHOR: L. GE (e-mail: leige@szu.edu.cn)

This work was supported by the Shenzhen Science and Technology Innovation Commission under Grant JCYJ20170818093035338.

**ABSTRACT** A beamwidth reconfigurable linear array antenna utilizing three magneto-electric (ME) dipole antenna elements with no need for a complex feeding network is presented. In this design, the ME dipole antenna elements are differentially excited by three parallel transverse resonant slots etched on the broad wall of a substrate integrated waveguide (SIW) cavity. By symmetrically embedding four copper posts that are connected to varactor diodes between the adjacent slots, the electric field perturbation in the SIW cavity can be realized by manipulation of the varactors. In other words, altering bias voltage of all the varactors simultaneously could offer granular control over the excitation amplitude and phase of the antenna elements. Consequently, continuously variable beamwidth of the antenna can be obtained under electronic control. A fully operational prototype was designed, fabricated, and tested to validate the proposed design. Measured results indicate that the overlapped −10 dB impedance bandwidth of the proposed antenna is 19.6% and the half-power beamwidth (HPBW) in the E-plane is capable of varying from 39° to 107° within the operating frequency band.

**INDEX TERMS** Beamwidth reconfigurable antenna, magneto-electric (ME) dipole, substrate integrated waveguide (SIW), varactor diode.

## I. INTRODUCTION

PATTERN reconfigurable antennas have been extensively used in wireless communication systems during the past few decades, for their high security, interference suppression, and large coverage area. A great deal of research has been conducted on the realization of scanning-beams [1], [2] or steerable-beams [3]–[5]. Another typical case is that the radiation pattern can be switched between unidirectional mode and omnidirectional mode [6], [7]. But when it comes to mobile communication systems, dynamic beamwidth control is commonly directed at base stations to improve the traffic capacity for different cells. For instance, when the base-station antennas are located in a relatively dense urban area, it is recommended that the radiation beamwidth be set to about 65° to decrease pilot pollution caused by a comparatively small station spacing, whereas if they are based in a suburban, the beamwidth then should be adjusted to around 120° for a large coverage area. Besides that, for the scenario of expressway or cross-sea bridge, the beamwidth is required to narrow down to 30° or so, with the purpose of covering a longer distance and restraining interference. Furthermore, with the rapid progress of city construction, the next generation cellular network environment changes frequently. Under such circumstances, in order to accommodate the needs and requirements of a variety of purposes and application scenarios, an installed base station antenna should be easy to achieve a dynamic continuous variation of the beamwidth.

According to the existing literature, beamwidth reconfigurable antennas could be implemented in several different methods. The most stereotypical way required

some mechanical movements, namely, manually adjusting distances between an RF feed horn and its reflectors [8] or moving metallic flaps of a bended H-sectoral horn antenna [9]. This would lead to some inevitable problems such as a lot of motion waste and a low alignment precision. As an option, to electronically control the beamwidth, the method of designing an antenna array configured with a switchable feeding network was adopted [10]. In this way, the number of the operative elements was selective, so the radiation direction and the beamwidth could change accordingly. But this was accompanied by a complex feeding network and a dramatic increase of the number of elements when a wider beamwidth adjustable range was desired. Alternatively, a solution based on the electronic control of the beamwidth using a partially reflective surface (PRS) antenna was proposed [11], [12]. The reconfiguration was accomplished by varying the reflectivity of the PRS through embedded varactor diodes or microelectro mechanical system (MEMS) switches. However, an extremely narrow bandwidth of about 1.5% and its complex structure restricted the practical application of this kind of antenna.

Recently, some promising beamwidth reconfigurable designs adopting magneto-electric (ME) dipole antennas with good performance have been reported [13]–[16]. Based on the different reconfiguration mechanism, they can be classified into two categories: a three-element ME dipole antenna array configured with a switchable feeding network [13], or a single ME dipole antenna with artificially introduced tunable components [14]–[16]. In [13], the half-power beamwidth (HPBW) could switch between 37° and 136° within a 15% fractional frequency band, as it was limited to the only two types of excitation phase distribution. To enhance the impedance bandwidth and the beamwidth variability, several sets of tunable strip gratings were assembled on the ground plane of an ME dipole antenna, resulting in an H-plane HPBW ranges from 81° to 153° covering a 40% impedance band [14]. Nonetheless, a large amount of p-i-n diodes (90 in total) kept the design away from a simple installation and operation. The remaining designs placed some tunable parasitic dipoles [15] or tunable parasitic patches [16] on the sides of a driven ME dipole, therefore, a continuous beamwidth reconfiguration was realized by tuning the bias voltage of a varactor diode loaded in each parasitic element. However, their narrowest H-plane HPBW was as wide as 80°, and so might not be employed in some special scenarios such as road tunnels or long span bridges.

Here we propose a new reconfigurable beamwidth ME dipole antenna configured with three aperture-coupled ME dipole elements, four post-loaded varactors embedded in the underneath substrate integrated waveguide (SIW) slotted-cavity. By altering the junction capacitance of the varactors at specific positions between the adjacent slots, the excitation amplitude and phase distribution of the array antenna is adjustable via just one dc power supply, thus the proposed antenna can continuously vary the E-plane beamwidth. Besides, the bias circuits of the varactors are built on the bottom surface of the SIW so that no dc wire is soldered on the upper surface, then their consequent negative impact on the radiation performance can be minimized. The proposed ME dipole antenna was fabricated and experimentally verified, indicating the antenna has an HPBW tuning range from 39° to 107° cover a 19.6% impedance band.

## II. ANTENNA DESIGN AND OPERATION PRINCIPLE

### A. GEOMETRY

The geometry of the proposed ME dipole array antenna is illustrated in Fig. 1. The antenna is mainly composed of three typical ME dipoles, a SIW slotted-cavity, and four copper posts connected to varactors. The ME dipole antenna, inspired by the concept of the complementary antenna consisting of an electric dipole and a magnetic dipole with perpendicular orientation and co-phase excitations [17], [18], is selected as the radiation element owing to the merits of wide bandwidth, unidirectional radiation, and stable beamwidth [19], [20]. As depicted in Fig. 1, each dipole comprises four horizontal metallic patches, four vertical metallic columns, and a crossed strip connecting the inner corners of the four patches for good impedance matching [21]. A 0.787-mm-thick substrate with relative permittivity of 2.33 is used to print the patches and the strips. The triple-dipole elements are integrated onto a 3.175-mm-thick Rogers laminate ($\varepsilon_r = 2.33, \tan\delta = 0.0012$) with a box-shaped reflector. Unlike the Γ-probe fed ME-dipole antenna that is commonly used, the proposed dipole elements are separately excited by three transvers slots situated on the upper metal surface of a SIW cavity. Moreover, they are differentially fed by two coaxial probes within the cavity to obtain a symmetrical radiation pattern in the H-plane.

The bottom rectangular SIW cavity is constituted with four arrays of metallized via-holes with uniform spacing. Those conducting vias act as metal sidewall of the cavity, so the diameter $dv$ and spacing $Sv$ of the vias should meet the requirement of $dv/Sv = 0.5$ and $dv/\lambda_0 = 0.1$ to prevent energy leak, where $\lambda_0$ is the free-space wavelength [22], [23]. Afterwards, three parallel rectangular slots are placed on the upper surface of the cavity with an element spacing of about $0.5\lambda_0$. The length $Ls$ of the resonant slot is set to approximately half wavelength of the operating frequency in the substrate. For a conventional SIW cavity-backed slot antenna structure, $TE_{120}$ mode is commonly served as the dominant mode. In this context, the proposed three-element linear array is composed of three slots, thus $TE_{160}$ mode is the associated dominant mode in the rectangular SIW cavity. As we know, for a rectangular SIW resonant cavity, the approximate values of the equivalent length $L_{eff}$ and width $W_{eff}$ are determined by:

$$f_{mn0} = \frac{c}{2\sqrt{\mu_r \varepsilon_r}} \sqrt{\left(\frac{m}{W_{eff}}\right)^2 + \left(\frac{n}{L_{eff}}\right)^2} \tag{1}$$

where $f_{mn0}$ denotes the eigenmode frequency, $\mu_r$ and $\varepsilon_r$ are the relative permeability and permittivity of the substrate, $c$ is

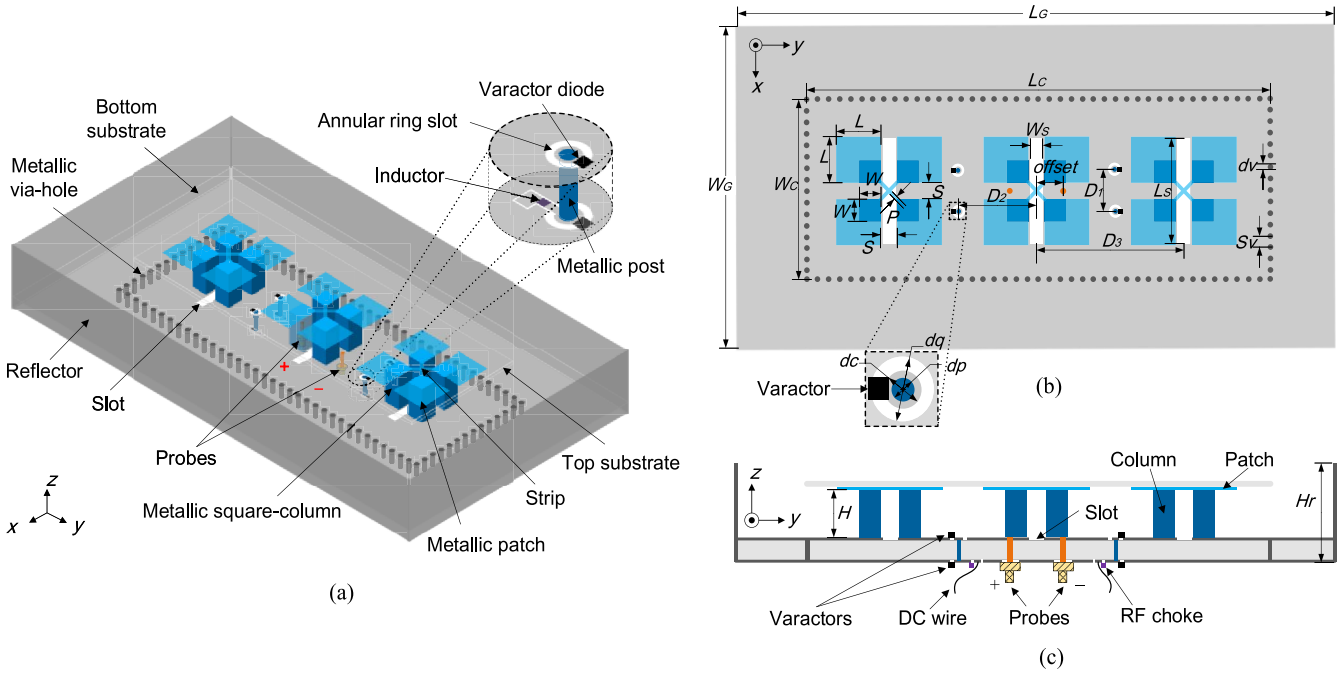


**FIGURE 1.** Geometry of the proposed beamwidth reconfigurable ME dipole antenna: (a) 3-D view; (b) top view; (c) sectional view.

**TABLE 1.** Key antenna parameters (in MM).

| Parameter | $W_G$ | $L_G$ | $Hr$ | $W_C$ | $L_C$ | $W$ | $L$ |
|---|---|---|---|---|---|---|---|
| Value | 130 | 242 | 30 | 68 | 182 | 9.4 | 18.8 |
| Parameter | $H$ | $S$ | $P$ | $Ws$ | $Ls$ | $offset$ | $D_1$ |
| Value | 18.8 | 4.8 | 1.4 | 4 | 41 | 10 | 16 |
| Parameter | $D_2$ | $D_3$ | $dp$ | $dc$ | $dq$ | $dv$ | $Sv$ |
| Value | 33 | 58 | 0.8 | 1.7 | 4.6 | 0.8 | 1.6 |

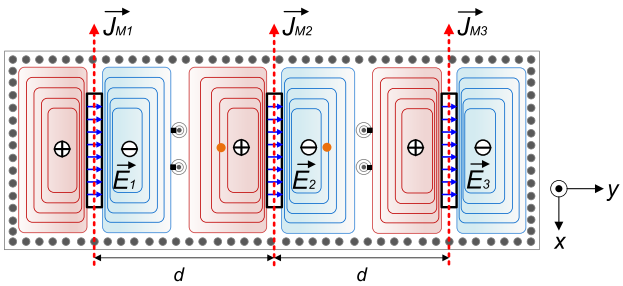


**FIGURE 2.** Electric field isoline of $TE_{160}$ mode in the SIW slotted-cavity of the proposed antenna.

the light velocity of free space, $m$ and $n$ refer to the numbers of variations in the standing wave pattern along the $x$- and $y$-axis directions, respectively. Based on the above analysis, the initial dimensions of the slots and the SIW cavity can be determined. The configuration of the copper posts and the varactors will be explained in Sections II-C and II-D. The detailed dimensions of the proposed antenna are tabulated in Table 1.

### B. THREE-ELEMENT ARRAY MODEL

As mentioned above, the three slots are designed to act as resonant slots, then $TE_{160}$ resonant mode can be generated in the SIW cavity, which can be seen in Fig. 2. The transverse electric fields, represented as blue short arrows, arise at the long edges of the slots along the $y$-axis. Accordingly, the corresponding equivalent magnetic currents flow along their vertical edges, represented by red dashed arrows. Ignoring the effect of the post-loaded varactors, the three magnetic current densities are supposed to have uniform amplitude. In this case, since the superstratum dipoles are excited by those slots respectively, the proposed antenna can be regarded as a three-element linear array, and the main lobe of the array points to the broadside direction with a relatively narrow HPBW.

As illustrated in Fig. 3, the total radiation pattern of a three-element linear array in the H-plane can be represented as [24]:

$$\begin{aligned} F(\theta)_T &= \mathrm{AF} \times f(\theta) \\ &= \left[a_1 e^{-j(kr_1+\Psi_1)} + a_2 e^{-j(kr_2+\Psi_2)} + a_3 e^{-j(kr_3+\Psi_3)}\right] f(\theta) \end{aligned} \tag{2}$$

where AF is the array factor, $f(\theta)$ is the radiation pattern of a single antenna element, and $a_n$ and $\Psi_n$ $(n = 1, 2, 3)$ are the excitation amplitude and phase of the elements, respectively. It is well known that the uniform amplitude distribution and the progressive phase difference between the elements are commonly used in the conventional scanning phased

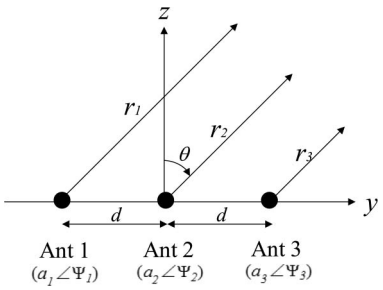


**FIGURE 3.** Three-element linear array model.

arrays. But for the operation of the beamwidth reconfiguration, the amplitudes and phases of the bilateral elements should be identical, but are different from that of the center element [13]. Assuming $a_2 = Ra_1 = Ra_3$, $\Psi_2 = \Psi_1 + \beta = \Psi_3 + \beta$, so the array factor turns into

$$\mathrm{AF} = a_1\left[2\cos(kd\sin\theta) + R\cos\beta - jR\sin\beta\right]. \tag{3}$$

Any variation in the amplitude ratio $R$ and/or the phase difference $\beta$ between the side elements and the center element will change the array factor, hence influencing the radiation beamwidth.

### C. RECONFIGURATION PRINCIPLE

For one thing, the desired nonuniform amplitude distribution of the elements, namely, diverse amplitude ratios $R$, can be realized by strategically introducing a number of post-loaded varactor diodes into the bottom feed layer. Moreover, these varactors arranged at selected positions can also change the excitation phase distribution as well.

To control the excitation amplitudes of the three elements and avoid considerably changing the resonant mode in the cavity, we place four conductive posts connected to varactors in the area of weak field in pairs. As you can see from Fig. 1(b) and Fig. 2, the four posts are symmetrical with respect to the center slot, and every pair of them are sandwiched between two adjacent slots. Specifically, altering the longitudinal separation between the posts and the middle slots $D_2$, has a great influence on the resonance occurred in the cavity. But the change in the transversal spacing of the posts $D_1$ has a relatively small impact and $D_1$ is tweaked to acquire appropriate insertion loss.

To better illustrate the effect of the post-loaded varactors, the E-field distributions in the SIW cavity with and without the varactors are shown in Fig. 4. For the case without the varactors, the E-field intensity distributions of the three slot-resonances appear nearly identical (see Fig. 4(a)), thus it can be approximately regarded as a uniform amplitude three-element array that yields the smallest HPBW [24]. If we embed the varactors into the cavity at the selected locations and set their capacitances $Cv$ as low as 1.1 pF, as shown in Fig. 4(b), the difference of the E-field intensity between the side slot resonance and the middle one increases a little, but is still comparatively small, implying a small variation in the amplitudes of the three elements. In consequence,

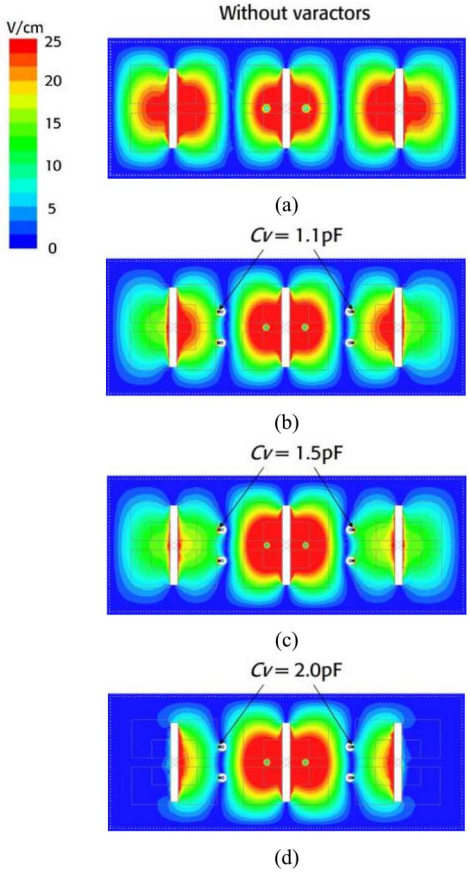


**FIGURE 4.** Electric field distributions in the SIW slotted-cavity (a) without the varactors, and with the varactors for different Cv at 2.5 GHz: (b) $Cv$ = 1.1 pF; (c) $Cv$ = 1.5 pF; (d) $Cv$ = 2.0 pF.

the corresponding beamwidth in the H-plane increases a little bit. As Fig. 4(c) shows, when $Cv$ continues to increase, significant different field intensity distributions within the resonant cavity can be observed, especially for the side elements. From Fig. 4(d), if $Cv$ is increased to 2.0 pF, the associated resonance within the cavity turns out to be quasi-$\mathrm{TE}_{140}$ mode. The slots on both sides perform like half-mode resonant slots since the lateral E-field strength is vanishingly small. That is, due to the effect of the varactors, the E-field magnitude distribution in the cavity can be greatly affected. As a result, such a great disparity in the amplitude between the side elements and the center one leads to an even wider beamwidth in the H-plane.

Next, let us move on to the mechanism of varying phase distributions of the antenna array (i.e., diverse phase differences $\beta$). If we insert a copper post in a section of the SIW transmission line, as shown in Fig. 5(a), it is equivalent to a T-network, which is given for illustration purpose only. The normalized reactance $X$ stands for the capacitive coupling effect between the post and the narrow metal wall of the SIW, whereas the normalized susceptance $B$ is brought by the inductive post [25].

In the process of traditional phase shifter designs, varactors or p-i-n diodes are commonly adopted to produce phase

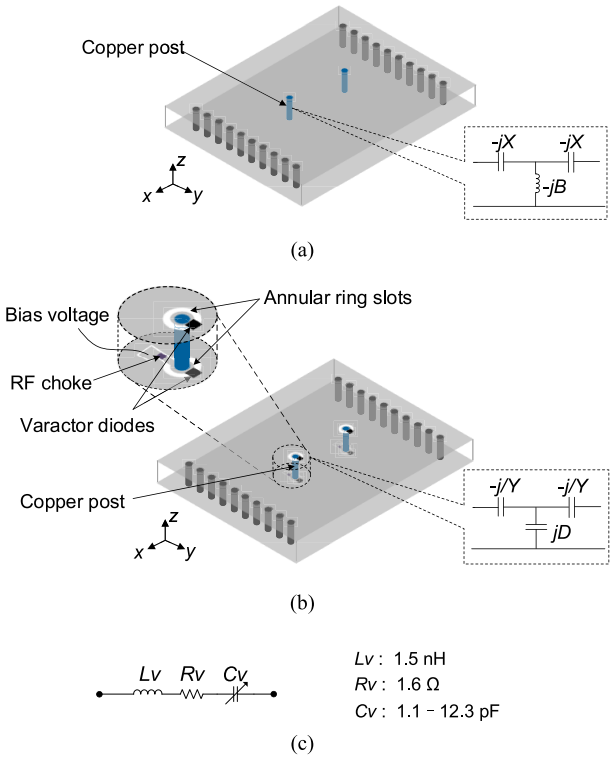


**FIGURE 5.** Simplified circuit networks of (a) the post, (b) the post connected with varactors embedded in the SIW, and (c) the varactor.

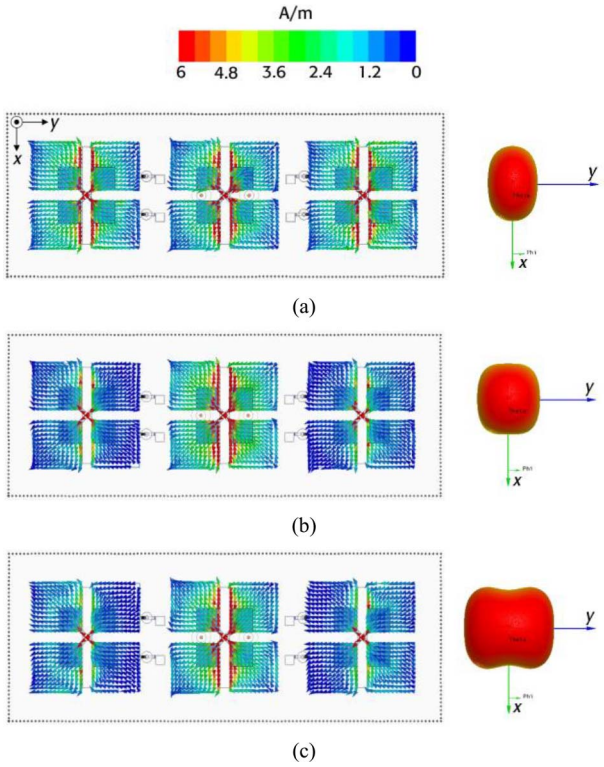


**FIGURE 6.** Current distributions on the horizontal patch, and 3-D radiation patterns of the proposed antenna with different *Cv* at 2.5 GHz. (a) *Cv* = 1.1 pF; (b) *Cv* = 1.5 pF; (c) *Cv* = 2.0 pF.

differences [25], [26]. So we add varactors onto the upper and lower surfaces of the SIW separately and connect them with the copper post, as shown in Fig. 5(b). Note that the both surfaces of the SIW are etched with annular ring slots around the post for proper installation of the varactors. After making this change, the post connected to varactors still can be identified with a T-network, but the normalized susceptance $D$ becomes the capacitive load between the broad wall of the SIW, which is generated by the parallel capacitance of the aforementioned varactors. The phase shift $\theta$ caused by the varactors can be derived from [26]:

$$\theta = \tan^{-1}\left[\left(-Y + \frac{2}{D} + \frac{1}{Y}\right)/\left(2 \times \left(\frac{Y}{D} + 1\right)\right)\right] \quad (4)$$

where the normalized reactance $Y$ is invariable as the position of the posts is fixed. Therefore, we can infer that the phase distribution changes with the different capacitance of the varactors.

### D. DESIGN ARGUMENT

In order to verify its feasibility, we chose the varactor diode, model *Skyworks SMV2023-011LF*, as the tunable component. According to the datasheet given in [27], its equivalent circuit model is given in Fig. 5(c). If we regulate its bias voltage from 20 to 0V, the corresponding capacitance *Cv* can vary from 1.1 to 12.3 pF. Additionally, cathodes of the varactors are soldered to the posts and connected to the positive terminal of a dc power supply via dc wires. Naturally, anodes

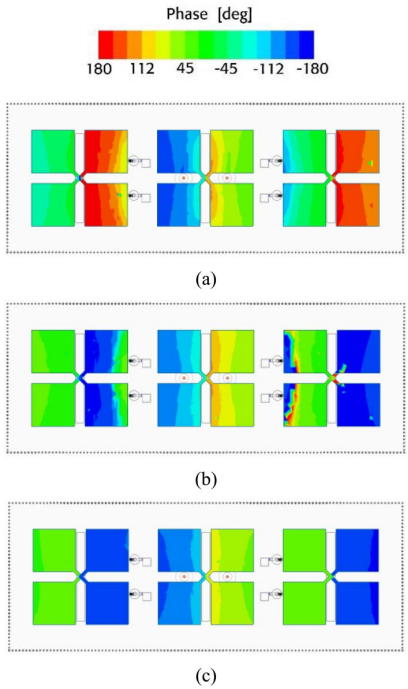


**FIGURE 7.** Phase distributions of E-field on the horizontal patch with different *Cv* at 2.5 GHz. (a) *Cv* = 1.1 pF; (b) *Cv* = 1.5 pF; (c) *Cv* = 2.0 pF.

of the varactors are soldered to the metal surface of the SIW and connected to the ground terminal of the dc power supply. Also noteworthy is that some dc contact pads surrounded

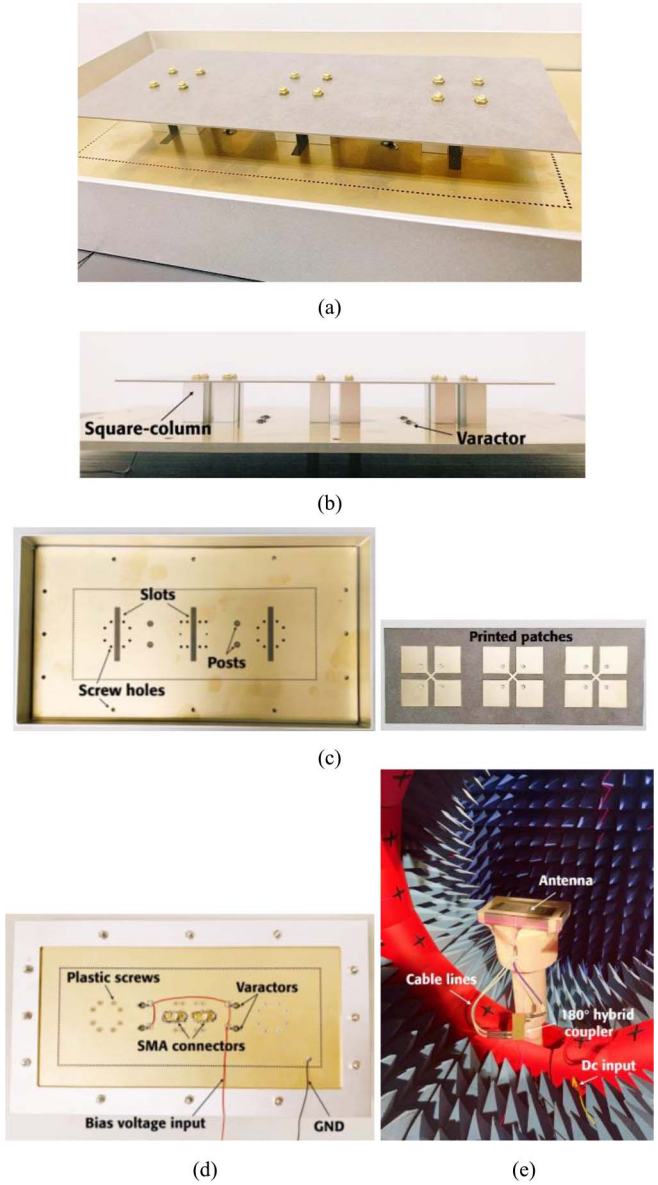


**FIGURE 8.** Photographs of the fabricated beamwidth reconfigurable antenna. (a) 3-D view, (b) side view, (c) unassembled laminates, (d) bottom view, (e) measurement setup in anechoic chamber.

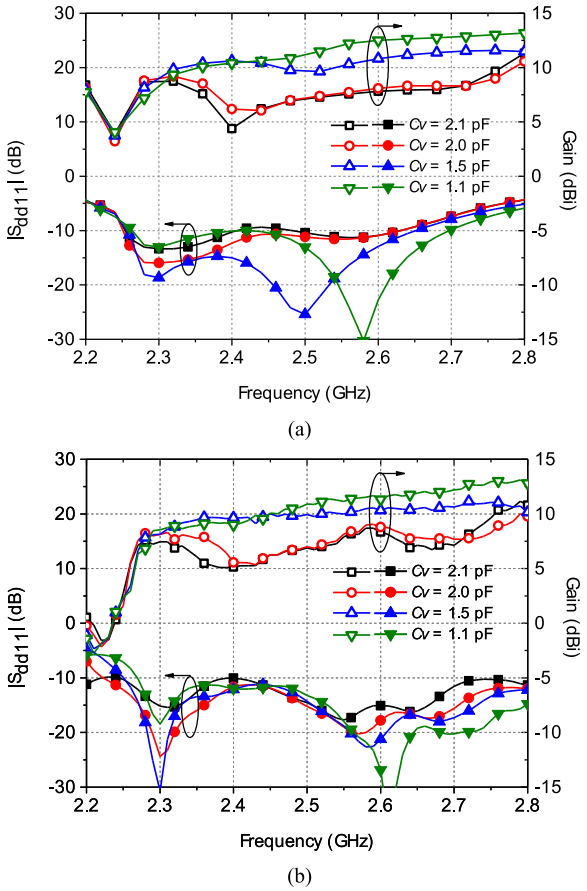


**FIGURE 9.** Simulated and measured reflection coefficients and peak gains of the proposed antenna with different *Cv*. (a) simulated results; (b) measured results.

by isolation slits on the bottom surface are intended for dc isolation of the varactors, as can be seen in Fig. 5(b). We select inductors of 47-nH, model *Murata LQW18A*, as the RF choke, and place them between the dc pads and the post-loaded varactors.

The surface current distributions on the horizontal dipoles with different *Cv* are shown in Fig. 6. When *Cv* varies from1.1 to 2.0 pF, the difference of the electric current density between the side dipoles and the center one is increased remarkably. And it is worth noting that there is very little change on the current intensity of the center dipole, whereas those of the side dipoles have undergone noticeable changes as *Cv* increases. The three-dimensional radiation patterns with varying *Cv* at 2.5 GHz can also be seen in Fig. 6. It indicates that the E-plane beamwidth gradually increases as *Cv* increases, whereas the H-plane beamwidth keeps almost unchanged. Besides, the phase distributions of the E-field on the patch with different *Cv* are plotted in Fig. 7. It can be seen that there is a gradual shift in the phases of the antenna elements when *Cv* is increased step by step. Consequently, by jointly varying the excitation amplitude and phase distribution of the three-element array, the synthesized radiation pattern can be electronically controlled by altering *Cv*.

## III. SIMULATED AND MEASURED RESULTS

Simulation was carried out using Ansys HFSS [28]. To verify the proposed design, a fully functional prototype was fabricated, as shown in Fig. 8. To facilitate the assembly of the antenna, some screw holes were drilled in the laminates, and plastic screws were used in the bottom laminate that had little effect. In addition, a 180° hybrid coupler was adopted to implement the differential feed of the proposed antenna, as can be seen in Fig. 8(e). Reflection coefficients ($|S_{dd11}|$) were measured by a Keysight N5225A network analyzer, while antenna gains, radiation efficiencies, and far-field radiation patterns were obtained by a Satimo Starlab near-field measurement system.

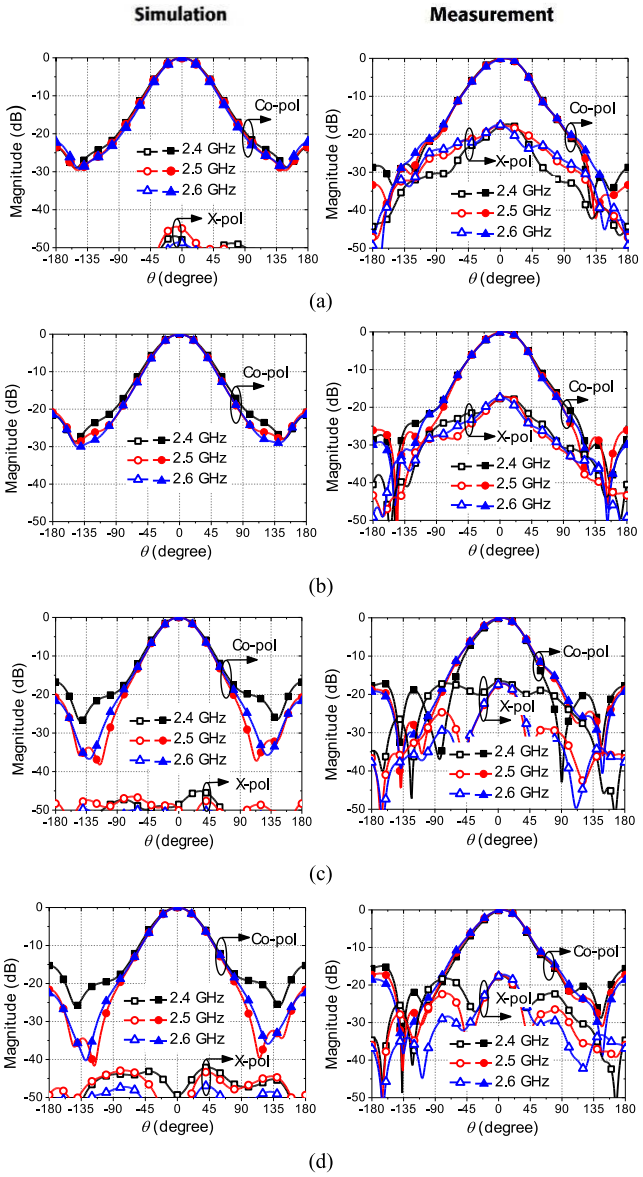


FIGURE 10. Simulated and measured radiation patterns in the H-plane with different *Cv*: (a) *Cv* = 1.1 pF; (b) *Cv* = 1.5 pF; (c) *Cv* = 2.0 pF; (d) *Cv* = 2.1 pF.

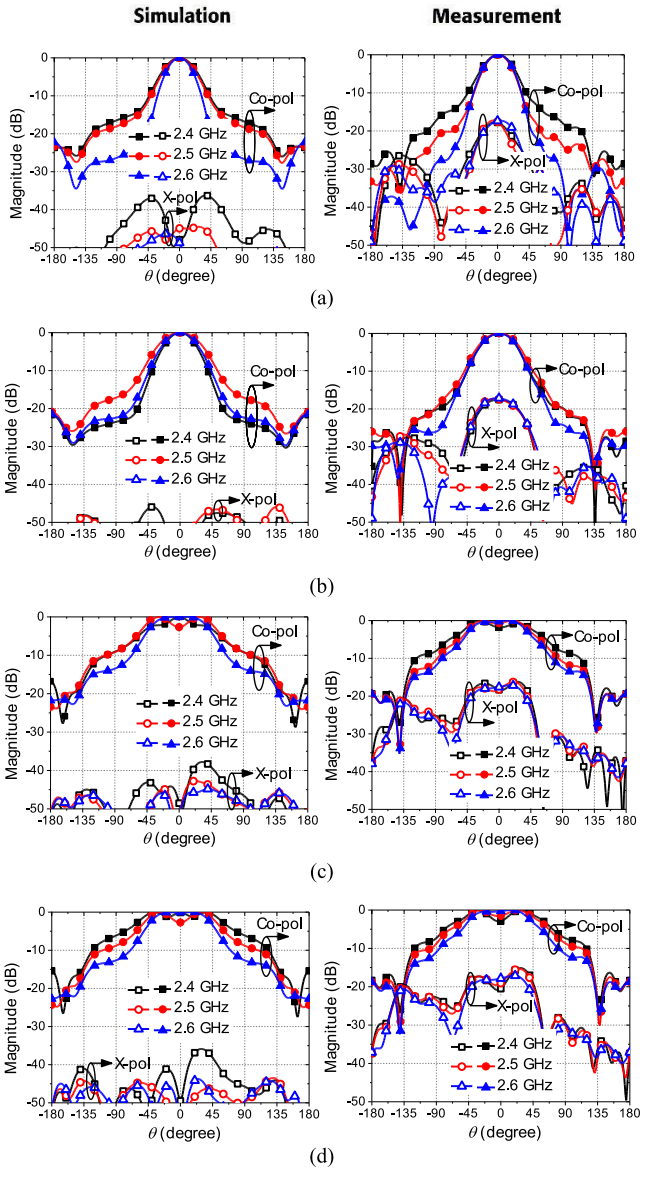


FIGURE 11. Simulated and measured radiation patterns in the E-plane with different *Cv*: (a) *Cv* = 1.1 pF; (b) *Cv* = 1.5 pF; (c) *Cv* = 2.0 pF; (d) *Cv* = 2.1 pF.

Simulated and measured differential reflection coefficients and peak gains of the proposed antenna under different capacitance values *Cv* of the varactors are plotted in Fig. 9. The measured reflection coefficients are with good agreement with the simulated ones. It is observed that the simulated broadside gain is as high as 12.6 dBi when *Cv* is 1.1 pF. But the peak gain drops to approximately 7.9 dBi when *Cv* is 2.1 pF. In essence, such a big discrepancy between the two states is due to the large E-plane beamwidth variation among them. The measured overlapped −10dB impedance bandwidth is about 19.6% from 2.26 to 2.75 GHz. It can be found that the impedance matching with different *Cv* is not completely consistent with each other. This can be attributed to the varying impedance of the antenna for diverse *Cv* from the standpoint of the equivalent circuit. From the figure, the measured broadside gains are slightly lower than the simulated results. The degradation

TABLE 2. Measured H-plane and E-plane HPBWs, peak gains, and efficiencies of the proposed antenna.

| Capacitance (pF) | H-plane HPBW (deg) | E-plane HPBW (deg) | Peak Gain (dBi) | Radiation Efficiency (%) |
|---|---|---|---|---|
| 1.1 | 58 ± 3 | 39 ± 2 | 11.1 ± 2.0 | 71 ± 2 |
| 1.5 | 57 ± 2 | 51 ± 3 | 9.9 ± 1.2 | 70 ± 3 |
| 2.0 | 55 ± 3 | 97 ± 10 | 7.7 ± 1.8 | 68 ± 1 |
| 2.1 | 55 ± 4 | 107 ± 14 | 7.4 ± 2.4 | 69 ± 2 |

**TABLE 3.** Comparison between the proposed and reported beamwidth reconfigurable antennas.

| Ref. | HPBW Variation Range (deg) | | HPBW Variation Ratio (%) | Operating Frequency (GHz) | Bandwidth ($\|S_{11}\|$< -10 dB) (%) | Peak Gain (dBi) | Dimension ($\lambda_0\times\lambda_0$) | Reconfiguration Mechanism |
|---|---|---|---|---|---|---|---|---|
| | H-plane | E-plane | | | | | | |
| [9] | 17-59 | N.A. | 347 | 2.9 | 1.5 | 10.7 | N.G. | Bended H-sectoral **horn** antenna with two movable metallic flaps |
| [10] | 31/45/65 | 15/20/35 | 3 states | 2.4 | 2.5 | 14.5 | N.G. | 3×6 **slot** array with switchable feeding network |
| [11] | 24-37 | 21-30 | 154; 143 | 2 | 1.5 | 14.4 | 3.3×3.3 | 10×10 **PRS** unit cells with 100 varactors |
| [12] | 16/39 | 16/34 | 2 states | 11.2 | N.G. | 14.7 | 6.7×6.7 | 18×18 **PRS** unit cells with 1296 MEMS elements |
| [13] | 37/136 | N.A. | 2 states. | 1.9 | 15 | 9.8 | 1.6×1.1 | 3-element **ME** dipole array with switchable feeding network |
| [14] | 81-153 | N.A. | 190 | 1.9 | 40 | 7.3 | N.G. | Tunable strip gratings of **ME** dipole antenna with 90 PIN diodes |
| [15] | 80-160 (LP); 72-133 (DP) | N.A. | 200; 185 | 2.0 | 10 | 7.1 | 1.2×1.2 (LP); 1.6×1.6 (DP) | Tunable parasitic dipoles of **ME** dipole antenna with 2 or 4 varactors |
| [16] | 80-120 | 65-120 | 185; 150 | 2.05 | 4.9 | 6.1 | 1.5×1.5 | Tunable parasitic patches of **ME** dipole antenna with 4 varactors |
| This work | N.A. | 39-107 | 274 | 2.5 | 19.6 | 11.1 | 2×1.1 | 3-element **ME** dipole array with tunable feeding structure (8 varactors) |

* $\lambda_0$ represents the free-space wavelength in the center operating frequency; N.A.: not applicable; N.G.: not given; LP: linear polarization; DP: dual-polarization.

of the measured results is basically caused by manufacturing and measuring errors.

Table 2 summarizes the measured peak gains of the proposed antenna within its operation band. We can see that the measured antenna gain is 11.1 ± 2.0 dBi when *Cv* is 1.1 pF. Then it declines to 7.4 ± 2.4 dBi when *Cv* increases to 2.1 pF. From the table, the measured radiation efficiencies are around 70% for different operation states.

When *Cv* is selected as 1.1, 1.5, 2.0, and 2.1 pF, in turn, the simulated and measured radiation patterns of the proposed antenna in the H-plane and the E-plane at frequency points of 2.4, 2.5, and 2.6 GHz are plotted in Fig. 10 and 11, respectively. It can be found that the H-plane radiation patterns are steady under different conditions, whereas the E-plane patterns vary dramatically when *Cv* changes. The measured HPBW in the H- and E-planes of the antenna are recorded in Table 2. It is noticeable that the H-plane HPBW is about 56° for different *Cv*. By contrast, the E-plane average HPBW is able to continuously vary from 39° (for *Cv* = 1.1 pF) to 107° (for *Cv* = 2.1 pF), which are in line with expectations. Besides, the trivial distinctions of the E-plane HPBWs in the same state at different frequencies are mainly caused by slight variations of the resonance within the SIW cavity.

In addition, the proposed antenna has unidirectional radiation patterns with the front-to-back ratio larger than 15 dB and the cross-polarization level lower than −17 dB over the working frequency range. It can be seen that good agreement is achieved between the simulated and measured results except for the cross-polarization level. During the simulation, it is found that the dc bias network does not affect the impedance matching and the gain of the antenna, but it interferes slightly with the cross polarizations. The simulated cross- polarization levels are extremely small in different states. This is because the ideal differential feed in the simulation is able to offer two balanced inputs with equiamplitude but out of phase, then the cross-polarization level is prominently lowered. But during the measurement, the practical 180° hybrid coupler and cables exposed in the radiation field, had a detrimental effect on the antenna performance, thus the measured results are worse than the simulated ones. Moreover, the phase tolerance caused by the coupler also aggravates their degradation.

Lastly, the performance of this work is summarized in Table 3 to compare with the reported beamwidth reconfigurable antennas. The sector horn antenna presented in [9], could vary H-plane HPBW from 17° to 59°. Its reconfiguration strategy was moving two flaps mechanically, which has the drawbacks of low accuracy and narrow bandwidth. As for the arrays with switchable feeding networks proposed in [10] and [13], the associated HPBWs could only be switched between three and two states respectively. Thus this might impede their extensive application in the complex and dynamic communication scenarios. Two PRS antennas were put forward in [11] and [12], the H- and E-plane beamwidth control were accomplished by integrating varactors or MEMS elements with the PRS unit cell. However, the complexity and massive usage of switches would cause many inconveniences to practical applications.

It can be found that the designs utilizing ME dipole structure show the superiority of wide bandwidth compared to the others. The ME dipole antenna with six tunable strip gratings proposed in [14] has a wide bandwidth of 40% and an HPBW variation range from 81° to 153°, but the excessive usage of PIN diodes remains a major problem. The

ME dipole antennas using tunable parasitic dipoles presented in [15], offering an additional design option for the polarization diversity. And its HPBW variation range covers from 80° to 160 ° in the H-plane with a 10% impedance bandwidth. Similarly, another ME dipole antenna adopting parasitic patches could vary its HPBW in both the E-plane (65°-120°) and the H-plane (80°-120°) with a 4.9% impedance bandwidth [16]. Compared with [15] and [16], this work has a higher HPBW variation ratio of up to 274%, a greater peak gain of 11.1 dBi, and a higher overlapping bandwidth of 19.6%, but a slightly larger dimension than [15].

## IV. CONCLUSION

A simple three-element ME dipole linear array antenna with beamwidth reconfiguration in the E-plane has been developed using the proposed methodology. The antenna elements are driven by three slots etched on the bottom SIW cavity. Without designing a complex feeding network, different amplitude and phase distribution of the array antenna is realized by tuning some post-loaded varactors embedded in the cavity. Only one dc signal is required to dynamically control the beamwidth. A 19.6% impedance bandwidth for $|S_{dd11}| < -10$ dB is realized, unidirectional radiation patterns with the cross-polarization level lower than $-17$ dB and the back radiation level lower than $-15$ dB are achieved in all operation states. The E-plane HPBW can continuously vary from 39° to 107°. With the features of simplicity in principle and setup, ease of control, and a wide adjustable beamwidth range, the proposed antenna is qualified to meet the requirements of flexible coverage of mobile communication systems.

## REFERENCES

[1] J. J. Luther, S. Ebadi, and X. Gong, "A low-cost 2×2 planar array of three-element microstrip electrically steerable parasitic array radiator (ESPAR) subcells," *IEEE Trans. Antennas Propag.*, vol. 62, no. 10, pp. 2325–2336, Oct. 2014.

[2] A. Khidre, F. Yang, and A. Z. Elsherbeni, "Circularly polarized beam-scanning microstrip antenna using a reconfigurable parasitic patch of tunable electrical size," *IEEE Trans. Antennas Propag.*, vol. 63, no. 7, pp. 2858–2866, Jul. 2015.

[3] G. H. Huff and J. T. Bernhard, "Integration of packaged RF MEMS switches with radiation pattern reconfigurable square spiral microstrip antennas," *IEEE Trans. Antennas Propag.*, vol. 54, no. 2, pp. 464–469, Feb. 2006.

[4] J. Ouyang, Y. M. Pan, and S. Y. Zheng, "Center-fed unilateral and pattern reconfigurable planar antennas with slotted ground plane," *IEEE Trans. Antennas Propag.*, vol. 66, no. 10, pp. 5139–5149, Oct. 2018.

[5] Q.-Y. Guo and H. Wong, "Wideband and high-gain fabry–pérot cavity antenna with switched beams for millimeter-wave applications," *IEEE Trans. Antennas Propag.*, vol. 67, no. 7, pp. 4339–4347, Jul. 2019.

[6] S.-L. S. Yang and K.-M. Luk, "Design of a wide-band l-probe patch antenna for pattern reconfiguration or diversity applications," *IEEE Trans. Antennas Propag.*, vol. 54, no. 2, pp. 433–438, Feb. 2006.

[7] X. J. Yang, H. W. Lin, H. Gu, L. Ge, and X. R. Zeng, "Broadband pattern diversity patch antenna with switchable feeding network," *IEEE Access*, vol. 6, pp. 69612–69619, 2018.

[8] H. Luh, "Variable beamwidth and zoom contour beam antenna systems," U.S. Patent 6 414 646 Jul. 2, 2002.

[9] A. Jouade, M. Himdi, A. Chauloux, and F. Colombel, "Mechanically pattern-reconfigurable bended horn antenna for high-power applications," *IEEE Antennas Wireless Propag. Lett.*, vol. 16, pp. 457–460, 2017.

[10] H. N. Chu and T.-G. Ma, "Beamwidth switchable planar microstrip series-fed slot array using reconfigurable synthesized transmission lines," *IEEE Trans. Antennas Propag.*, vol. 65, no. 7, pp. 3766–3771, Jul. 2017.

[11] T. Debogovic, J. Perruisseau-Carrier, and J. Bartolic, "Partially reflective surface antenna with dynamic beamwidth control," *IEEE Antennas Wireless Propag. Lett.*, vol. 9, pp. 1157–1160, 2010.

[12] T. Debogovic, J. Bartolić, and J. P. Carrier, "Dual-polarized partially reflective surface antenna with MEMS-based beamwidth reconfiguration," *IEEE Trans. Antennas Propag.*, vol. 62, no. 1, pp. 228–236, Jan. 2014.

[13] L. Ge and K.-M. Luk, "A three-element linear magneto-electric dipole array with beamwidth reconfiguration," *IEEE Antennas Wireless Propag. Lett.*, vol. 14, pp. 28–31, 2015.

[14] L. Ge and K.-M. Luk, "Beamwidth reconfigurable magneto-electric dipole antenna based on tunable strip grating reflector," *IEEE Access*, vol. 4, pp. 7039–7045, 2016.

[15] L. Ge and K.-M. Luk, "Linearly polarized and dual-polarized magneto-electric dipole antennas with reconfigurable beamwidth in the h-plane," *IEEE Trans. Antennas Propag.*, vol. 64, no. 2, pp. 423–431, Feb. 2016.

[16] Y. Shi, Y. Cai, J. Yang, and L. Li, "A magnetoelectric dipole antenna with beamwidth reconfiguration," *IEEE Antennas Wireless Propag. Lett.*, vol. 18, no. 4, pp. 621–625, Apr. 2019.

[17] A. Clavin, "A new antenna feed having equal e- and h-plane patterns," *Trans. IRE Prof. Group Antennas Propag.*, vol. AP-2, no. 3, pp. 113–119, Jul. 1954.

[18] K.-M. Luk and H. Wong, "A new wideband unidirectional antenna element," *Int. J. Microw. Opt. Technol.*, vol. 1, no. 1, pp. 35–44, 2006.

[19] H. Wong, K.-M. Mak, and K.-M. Luk, "Wideband shorted bowtie patch antenna with electric dipole," *IEEE Trans. Antennas Propag.*, vol. 56, no. 7, pp. 2098–2101, Jul. 2008.

[20] L. Siu, H. Wong, and K.-M. Luk, "A dual-polarized magneto-electric dipole with dielectric loading," *IEEE Trans. Antennas Propag.*, vol. 57, no. 3, pp. 616–623, Mar. 2009.

[21] Y. Li and K.-M. Luk, "60-GHz dual-polarized two-dimensional switch-beam wideband antenna array of aperture-coupled magneto-electric dipole," *IEEE Trans. Antennas Propag.*, vol. 64, no. 2, pp. 554–563, Feb. 2016.

[22] F. Xu and K. Wu, "Guided-wave and leakage characteristics of substrate integrated waveguide," *IEEE Trans. Microw. Theory Techn.*, vol. 53, no. 1, pp. 66–73, Jan. 2005.

[23] D. Deslandes and K. Wu, "Accurate modeling, wave mechanisms, and design considerations of a substrate integrated waveguide," *IEEE Trans. Microw. Theory Techn.*, vol. 54, no. 6, pp. 2516–2526, Jun. 2006.

[24] C. A. Balanis, *Antenna Theory: Analysis and Design*. New York, NY, USA: Wiley, 2005.

[25] K. Sellal, L. Talbi, and M. Nedil, "Design and implementation of a controllable phase shifter using substrate integrated waveguide," *IET Microw. Antennas Propag.*, vol. 6, no. 9, pp. 1090–1094, Jun. 2012.

[26] H. Peng, P. Jiang, T. Yang, and H. Y. Jin, "Continuously tunable SIW phase shifter based on the buried varactors," *IEICE Electron. Exp.*, vol. 12, no. 7, pp. 1–7, Apr. 2015.

[27] Skyworks Inc. *SMV2019 to SMV2023 Series: Hyperabrupt Junction Tuning Varactors*. [Online]. Available: https://www.skyworksinc.com/en/Products/Diodes/SMV2023-Series

[28] Ansys Corporation. *HFSS: High Frequency Structure Simulator Based on the Finite Element Method*. [Online]. Available: http://www.ansys.com

**YUAN JI** (Graduate Student Member, IEEE) was born in Jiangsu, China. She received the B.S. degree in information engineering from Southeast University, Nanjing, China, in 2009, and the M.S. degree in telecommunication engineering from the University of Melbourne, Melbourne, VIC, Australia, in 2011. She is currently pursuing the Ph.D. degree in electronic science and technology with the Nanjing University of Science and Technology, Nanjing.

Her current research interests include phased array antennas, base station antennas, reconfigurable antennas, and dielectric resonator antennas.

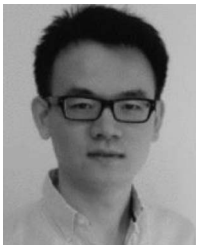

**LEI GE** (Senior Member, IEEE) was born in Jiangsu, China. He received the B.S. degree in electronic engineering from the Nanjing University of Science and Technology, Nanjing, China, in 2009, and the Ph.D. degree in electronic engineering from the City University of Hong Kong, Hong Kong, in 2015.

From September 2010 to July 2011, he was a Research Assistant with the City University of Hong Kong, where he was a Postdoctoral Research Fellow with the State Key Laboratory of Millimeter Waves from April 2015 to October 2015. He is currently an Assistant Professor with Shenzhen University, China. His recent research interests focus on patch antennas, base station antennas, reconfigurable antennas, MIMO antennas, millimeter-wave antennas, and multiband antennas. He received the Honorable Mention at the student contest of the 2012 IEEE APS-URSI Conference and Exhibition, Chicago, USA. He won the 1st Prize in the Student Innovation Competition of 2014 IEEE International Workshop on Electromagnetics, Sapporo, Japan, in 2014. He was a recipient of the IEEE Antennas and Propagation Society Outstanding Reviewer Award from 2017 to 2018. He was a TPC member and a session chair of several international conferences.

**JIANPENG WANG** received the Ph.D. degree from the University of Electronic Science and Technology of China, Chengdu, China, in 2007.

From 2005 to 2006, he was a Research Assistant with the Institute for Infocomm Research, Singapore. From 2010 to 2011, he was a Research Fellow with the School of Electrical and Electronic Engineering, Nanyang Technological University, Singapore. In 2013, he joined the School of Engineering and Physical Sciences, Heriot Watt University, Edinburgh, U.K., as a Visiting Scholar. From 2014 and 2016, he was a Research Fellow with the Faculty of Science and Technology, University of Macau, Macau, China. He is currently an Associate Professor with the School of Electronic and Optical Engineering, Nanjing University of Science and Technology, Nanjing, China. He has authored or coauthored over 90 papers in international journals and conference proceedings. His current research interests include microwave circuits, antennas, and LTCC-based millimeter-wave circuits.

Dr. Wang has been an Associate Editor of *IET Electronics Letters* since 2015.

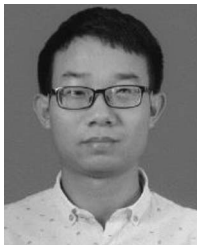

**QUANGANG CHEN** was born in Henan, China, in 1992. He received the B.S. degree in electronic information engineering and the M.S. degree in electromagnetic field and microwave technology from the Nanjing University of Science and Technology, Nanjing, China, in 2015 and 2018, respectively. He is currently pursuing the Doctoral degree with the Department of Electronics and Nanoengineering, School of Electrical Engineering, Aalto University.

From 2018 to 2019, he was a Research Assistant with the College of Electronic Science and Technology, Shenzhen University. His current research interests include multiband smartphone antennas and MIMO antennas.

**WEN WU** (Senior Member, IEEE) received the Ph.D. degree in electromagnetic field and microwave technology from Southeast University, Nanjing, China, in 1997.

He is currently a Professor with the School of Electronic and Optical Engineering, Nanjing University of Science and Technology, Nanjing, where he is also an Associate Director with the Ministerial Key Laboratory of JGMT. He has authored or coauthored over 300 internationally referred journal and conference papers and holds 14 patents. His current research interests include microwave and mm-wave theories and technologies, microwave and mm-wave detection, and multimode compound detection.

Prof. Wu was a six-time recipient of the Ministerial and Provincial-Level Science and Technology Award.